

# Cold Atom targets in the femtosecond laser field

Renyan Li,<sup>1,2</sup> Junyang Yuan,<sup>1,2,3</sup> Xinya Hou,<sup>4</sup> Shuai Zhang,<sup>1</sup> Zhiyuan Zhu,<sup>1,3</sup> Yixuan Ma,<sup>1,3</sup> Qi Gao,<sup>1</sup> Zhongyang Wang,<sup>1,3</sup> T.-M. Yan,<sup>1</sup> Matthias Weidemüller,<sup>5</sup> Xincheng Wang,<sup>3,6, a)</sup> Yizhu Zhang,<sup>1,7, b)</sup> and Yuhai Jiang<sup>1,2,3,4, c)</sup>

<sup>1)</sup> Shanghai Advanced Research Institute, Chinese Academy of Sciences, Shanghai 201210, China

<sup>2)</sup> University of Chinese Academy of Sciences, Beijing 100049, China

<sup>3)</sup> School of Physical Science and Technology, ShanghaiTech University, Shanghai 201210, China

<sup>4)</sup> Henan Normal University, Xinxiang 453007, China

<sup>5)</sup> Physikalisches Institut, Universität Heidelberg, Im Neuenheimer Feld 226, 69120 Heidelberg, Germany

<sup>6)</sup> Fudan University, Shanghai 200433, China

<sup>7)</sup> Tianjin University, Tianjin 300072, China

(Dated: 8 July 2022)

We have built up a magneto-optical trap (MOT) recoil ion momentum spectroscopy (RIMS) (MOTRIMS) apparatus for studies of Rb atom in strong infrared laser field. Three cold Rb target modes namely two-dimensional (2D) MOT, 2D molasses MOT, and 3D MOT can be provided in the setup and the profiles for the density and the velocity of 3D MOT are characterized using absorption imaging and photoionization approaches. The momentum distributions of  $\text{Rb}^+$  for three types of atom targets are detected with standard RIMS method and the resolution of 0.15 a.u. is achieved along the extraction direction.

## I. INTRODUCTION

In the past few decades, COLTRIMS (cold target recoil ion momentum spectroscopy),<sup>1-3</sup> which enables investigations of dynamical processes of ion-atom/ion-molecule and photon-atom/photo-molecule collisions in  $4\pi$  solid angle with a high resolution, becomes one of the most fruitful experimental techniques in the field of atomic, molecular and optical (AMO) physics. In the COLTRIMS, experimental targets are limited to the species of atoms/molecules in gas phase and volatilizable liquid, normally presented by a supersonic jet. It is very hard for usage of COLTRIMS-like apparatus to detect the recoil-ion momentum distributions of the alkali and alkaline-earth atoms because of their solid phase at room temperature. Meanwhile, for alkali atoms, the profiles of hydrogen-like and extremely low first-ionization energy result in an additional way to understand the field ionization dynamics. For instance time-resolved holography of photoelectrons reveals rich intra- and inter-cycle interferences,<sup>4</sup> where metastable xenon atoms were prepared. Instead of noble gas alkali atoms are ideal targets for study of photoelectron interferences, particularly for intermediate-involved states in the far- and mid-infrared laser field since alkali atoms can be easily prepared on various initial states with lasers. However heating alkali atoms to gas phase may lead to large thermal motion in the level of a couple of 10 a.u. so that it is impossible to detect recoil-ion of a few a.u. induced by the strong laser field with reasonable momentum resolu-

tion. Considering these species as target, the magneto-optical trap (MOT) technology has been introduced to the COLTRIMS, called as magneto-optical trap recoil ion momentum spectroscopy (MOTRIMS),<sup>5</sup> which enables Rb atom target to be cooled to the temperature in the order of 100  $\mu\text{K}$ , that is about three orders lower than supersonic expansion target in the temperature for comparable atomic mass. Targets in the extremely low temperature will result in unbelievable momentum resolution of recoil-ion.

Recently, MOTRIMS was employed for studies of photoionization with excitation of Li atom in the free electron laser radiations and infra-red strong laser field.<sup>6-8</sup> Later, MOTRIMS for Li atom in Heidelberg was extended successfully for exploring ion collision measurements<sup>9</sup>. Besides, MOTRIMS for Rb was build and performed in the research of the photoassociation of ultracold molecules.<sup>10-12</sup>

In this work, a new MOTRIMS for rubidium atom will be introduced, in which a pulsed femtosecond laser was used to ionize Rb atom for characterization of MOT. Three cold rubidium beams with 2D MOT, molasses MOT, and 3D MOT are provided in present setup. In 2D MOT, rubidium atoms in ground state cooled in two dimensions in glass cell are directed into science chamber via differential pipe. 2D MOT is considered to be 2D molasses MOT if it is cooled by cooling laser but without magnetic quadrupole field. For 3D MOT, the rubidium atoms are cooled further by six lasers in science chamber and trapped with magnetic quadrupole field leading to the highest density and same temperature in three dimensions. Three types of cold atom beams present different atom densities, target temperatures and initial states, resulting in various momentum resolutions for recoil ion which will be characterized and be discussed in details

<sup>a)</sup>Electronic mail: wangxc@sari.ac.cn

<sup>b)</sup>Electronic mail: zhangyz@sari.ac.cn

<sup>c)</sup>Electronic mail: jiangyh@sari.ac.cn

latter.

## II. EXPERIMENTAL SETUP

The setup consists of three parts, dubbed as the 2D MOT preparation,<sup>13–18</sup> 3D MOT target and recoil ion momentum spectrometer<sup>19,20</sup> respectively, this will be described in the following section. Rb atoms are pre-cool in two dimensions in 2D MOT preparation, then pushed in main chamber and further cooled by 3D MOT. And the ions generated in the process of the interaction between Rb atoms and femtosecond laser can be extracted and detected by recoil ion momentum spectrometer. In the 2D MOT preparation part, a glass chamber is set at the top of the main chamber, in which a rubidium dispenser is heated through a current of about 4A, and thus rubidium vapor can be generated. The quantity of vaped rubidium gas can be controlled by changing the current. The vaped rubidium atoms are pre-cooled in the glass chamber by cooling laser before pushed into the main chamber. Two cooling laser beams with red detuning of -12 MHz from  $|5S_{1/2}, F = 3, m_F = 3\rangle \rightarrow |5P_{3/2}, F'=4, m_{F'} = 4\rangle$  are split into four pairs of beams with perpendicular directions respectively. Each beam passes a  $1/4 \lambda$  plate to achieve circular polarization optics before entering the glass cell, then retro-reflected by a plane mirror. Another  $1/4 \lambda$  plate is set at the front of a plane mirror to achieve the reverse circular polarization as it should be. The 2D MOT preparation part can be separated from the main chamber via a gate valve. In the 3D MOT part, the rubidium atoms can be further cooled down by three pairs of orthogonal cooling lasers by detuned of -19 MHz from  $|5S_{1/2}, F = 3, m_F = 3\rangle \rightarrow |5P_{3/2}, F'=4, m_{F'} = 4\rangle$  and trapped by magnetic quadrupole field in 3D MOT. A femtosecond laser was used to ionize the target, offer a tool for characterization and further experiments. The femtosecond laser can interact either with 2D MOT beam directly or with 3D MOT. Besides, the rubidium target can be prepared with cooling laser but without magnetic quadrupole field, which is dubbed as optical molasses. The features such as atom density, temperature and initial state are different between different targets, namely 2D MOT, molasses and 3D MOT. Furthermore, as the magnetic quadrupole field will reduce the resolution of recoil ion momentum, the magnetic can be switch off shortly (about 20 ms) after the 3D MOT is loaded. This plan will be used only when it is necessary, since it will spend more experimental time. The 3D MOT target can maintain only about 20 ms after switching off the magnetic coils current and need about 500 ms to reload, so the highest efficiency is about 38 Hz while the repetition rate of our femtosecond laser is 1 kHz. The third part of the setup is a RIMS (recoil ion momentum spectroscopy) as detecting system in which the time of flight and the final position of ionized atoms from cold atom target will be measured through a 2D position sensitive MCP (Designed and produced by

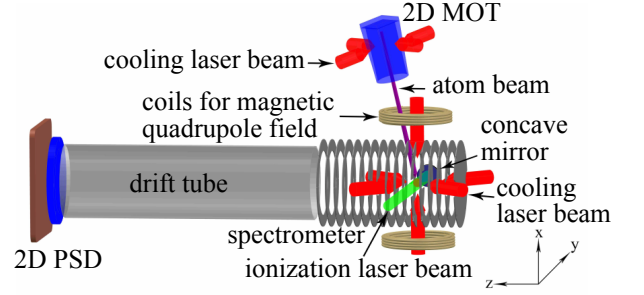


FIG. 1. The sketch of the MOTRIMS. In the 2D MOT preparation part, the atoms can be pre-cooled in two dimensions. In the 3D MOT part, the pre-cooled atoms can be further cooled in three dimensions. And the momentum of recoil ion can be detected with the third part, i.e. the RIMS. X, y, z -axis represent directions for 2D beam, femtosecond laser propagation and spectrometer longitude, respectively.

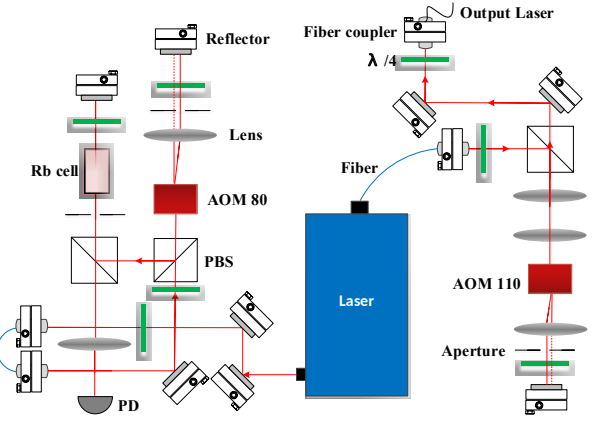


FIG. 2. Scheme of the laser system. AOM: acousto-optical modulators, PBS: polarization beam splitter, PD: Photo-Diode

RoentDek Handels GmbH) detector. Using these data more information about the interaction, such as momentum and kinetic energy of recoil ion, can be deduced. All the three parts of the setup will be described in detail in the following part in paper respectively.

### A. Laser system

The laser system provides 2D cooling, 3D cooling, pushing, imaging and repumping beams. The 2D cooling beam with a power of 130 mW used for pre-cooling the Rb atoms in two dimensions is split into two beams. The pushing beam with a power of 0.6 mW is used for push the pre-cooled Rb into the main chamber, where three branches of 3D cooling beam (60 mW in total) will further cool the Rb atoms down to  $\sim 100 \mu\text{K}$ . The repumping beam (14 mW in total) for 2D MOT and 3D MOT drives the  $F = 2 \rightarrow F' = 3$  transition, pumps the Rb atoms back into the cooling cycle. And the imaging beam is used in

the absorption imaging experiment to measure the characteristics of 3D MOT target which will be described in detail in Section III. Fig. 2 is the schematic design of the laser system. Laser beam on the left side which passes a Rb vapor cell is used for Doppler-free saturation spectroscopy<sup>21</sup>. An Acousto-optical Modulators(AOM) in a double-pass configuration shifts the frequency by  $2 \times 80$  MHz thus the laser beam can be locked on the  $F' = 3/4$  crossover. This part of the optical design can stabilize the working frequency of the laser beams on the right side. The optical paths of 2D cooling, 3D cooling, pushing and imaging beams are similar but with different detuning. So only one optical path is shown. The different detuning is also achieved by using an AOM in a double-pass configuration. Then the output laser beam is transported to the chamber by polarization-maintaining single mode optical fiber. Since the repumping light is on resonance to the  $F = 2 \rightarrow F' = 3$  transition, another laser system, similar to the laser system mentioned above is used. The repumping laser beams are locked on  $F = 2/3$  crossover (shifted by  $2 \times 110$  MHz), both for 2D and 3D MOT.

## B. 2D MOT preparation

Zeeman slower and 2D MOT are two traditional atom pre-cool schemes. However, compare with 2D MOT, Zeeman slower has two main difficulties to overcome. One problem is that the Zeeman slower has no cooling in transverse direction. The other problem is that either the laser is on resonance or the magnetic field has to be non-zero at the end of the Zeeman slower. This means that the MOT that normally sits at this position is either disturbed by the resonant light or the magnetic field of the slower<sup>22</sup>. Thus, the 2D MOT scheme is chose to pre-cool the atoms. The rubidium vapor is generated in a glass cell with a rubidium wire heated by a current between 2 A to 4 A. The rubidium atoms in the vapor is cooled and trapped into a beam by the cooling and repumping laser and a magnetic quadrupole field. As the cooling and repumping laser is split into four beams with a  $1/e^2$  diameter of 20 mm, the rubidium atom beam has four identical cooling regions with total length of 8 cm. As all the light mentioned above are introduced by polarization-maintaining single mode fibers and split into four beams by PBS (polarization beam splitter) before entering the glass cell through optical fiber couplers respectively. The cooling light is red-detuned by  $\delta = -2$   $\Gamma$ ,  $\Gamma = 6$  MHz being the natural linewidth from the  $|5S_{1/2}, F = 3, m_F = 3\rangle \rightarrow |5P_{3/2}, F'=4, m_{F'} = 4\rangle$  cooling transition and the repumping light is on resonant with the  $|5S_{1/2}, F = 2, m_F = 2\rangle \rightarrow |5P_{3/2}, F'=3, m_{F'} = 3\rangle$  transition. The atoms can be pre-cooled by these cooling and repumping lasers in two dimensions. A magnetic field gradient of 18 G/cm is generated by 6 pairs of permanent magnets set on two sides of the glass cell, which was optimized to get the best atom flux. Every piece of permanent magnet

can be adjusted independently to align the four cooling regions. All the optical fiber couplers and permanent magnets are set on a metal cage which is fixed around the glass cell. After cooling into 2D MOT in glass cell, the rubidium beam will be pushed into the main chamber through a hole with diameter of 800  $\mu$ m by a pushing beam set at one end of the glass cell. The pushing beam is red-detuned by -25 MHz and has a  $1/e^2$  diameter of 6 mm. The pushed atom beam can interact with ionization laser beam as atom target dubbed as 2D MOT.

## C. 3D MOT target

3D MOT atom target has higher atom density and cooler temperature compared with 2D MOT and molasses. Nevertheless, these forms of target may also be used for different types of experiments so as to increase the resolution of recoil ion momentum or for a proper count rate. Similar laser system as in 2D MOT is adopted. The cooling light in 3D MOT is red-detuned by -18 MHz from the  $|5S_{1/2}, F = 3, m_F = 3\rangle \rightarrow |5P_{3/2}, F'=4, m_{F'} = 4\rangle$  with  $1/e^2$  diameter of 20 mm. The repumping beams are on resonance with the  $|5S_{1/2}, F = 2, m_F = 2\rangle \rightarrow |5P_{3/2}, F'=3, m_{F'} = 3\rangle$  transition. cooling and repumping laser is split into three identical beams before conducted to the main chamber by polarization maintaining single mode fiber. Each laser beam comes from optical coupler passes through a  $1/4 \lambda$  plate, two viewports and the main chamber then get reflected by a  $1/4 \lambda$  plate and a plano mirror. All the incident beams and the reflected beams intersect in the center of the main chamber where the 3D MOT target will form. To trap the cold atoms in 3D MOT, the magnetic quadrupole field is generated by a pair of copper tube coils. The coils have a distance of 120 mm and each has an inner diameter of 35 mm and 16 turns. Cooling water passes through the center of the coil tube to protect them from damage of high temperature generated by electrical heating. A magnetic field gradient of 18 G/cm can be obtained with a current of about 47A.

## D. Recoil ion momentum spectrometer

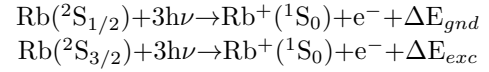
The recoil ion momentum spectrometer is a powerful instrument for detecting the momentum of recoil ion with 4 solid angle. The spectrometer in our setup consists of 35 pieces of stainless steel ring electrodes to extracting recoil ions from target to detector. Every electrode has the same thickness of 1 mm and all the distances between adjacent electrodes are 4 mm. The outer diameter of the electrodes are 100 mm and an inner diameter 75 mm except for the first piece on the repelling edge. The first piece is a disk with a diameter of 100 mm called repeller. The outermost two electrodes can be set at different voltages independently depending on the type of experiment. A uniform electric field is provided as all adjacent elec-

trodes are connected by resistors of the same resistance of 1 M. As for photoionization experiment, if not specified, an electric field of 0.52 V/cm is set with a voltage difference of 8.85 V to keep a balance between a better resolution of recoil ion momentum and a preferable efficiency. A drift tube with length of 670 mm and inner diameter of 81 mm is used to improve the resolution of recoil ion momentum. A commercial Z-stack MCP anode delay-line detector with an active area of 80 mm × 80 mm is used for recoil ion position detection in two dimensions. It should be pointed out that, as a cooling and repumping/ ionizing laser beam has a  $1/e^2$  diameter of 20 mm, the part of electrodes on the propagation path of the laser beams are removed, forming holes with diameter of 20 mm for the transmission of the laser. And parts from the same electrode are connected through thin wires, which will not block any of the light. The same is done also for the transmissions of 2D MOT atoms beam.

### III. CHARACTERIZATION OF THREE TYPES OF COLD ATOM TARGET

As mentioned above, the setup can work in three types of targets. In 2D MOT, the femtosecond will interact with atoms pre-cooled from 2D MOT. This atom target has lower atom density and worse recoil ion momentum resolution than the other two. In molasses, the pre-cooled atoms pushed into the main chamber will be further cooled by cooling laser. To get higher target density, in 3D MOT, the magnetic quadrupole generated by a pair of copper coils set at the top and bottom inside the main chamber should be added. Besides, the initial states of different targets are different as part of the atoms will be excited to excited state by the cooling light in molasses and in 3D MOT. In this section, we characterized three different types of targets, molasses, 2D MOT, 3D MOT include their momentum distribution in different directions and their resolutions correspondingly. Then the density profiles of the 3D MOT characterized will be described with two different methods, absorption imaging<sup>23</sup> and photoionization experiment.

In the photoionization experiment, the rubidium atoms are ionized from ground state or excited state using femtosecond laser pulse with wavelength of 800 nm at a repetition rate of 1 kHz. The output energy of the femtosecond laser is 2.7 mJ, then the energy can be adjusted using a calcite wollaston prism and a half-wave plates before entering the main chamber. The incident femtosecond laser beam is focused by the concave mirror mounted on the multi-axis manipulation. The dominant process is that an ionized rubidium atom absorbing two photons at least, result in non-resonant photoionization from ground state for the atoms without cooling laser and excited state for most of the atoms in the targets with cooling laser. As the cooling light can excite rubidium atoms in excited state. Then an excess energy  $\Delta E_{gnd} = 0.473$  eV or  $\Delta E_{exc} = 2.07$  eV is released:



Using the data of the position of recoil ions imaged in the MCP anode delay-line detector in two dimensions and the time of flight from atom target to the detector, the momentum of recoil ions in three dimensions can be calculated.

In order to obtain the characters of the 3D MOT target, such as the profile, the velocity and the temperature in different directions, photoionization experiment and absorption image experiment are performed. For the purpose of obtaining higher laser intensity to perform photoionization experiment, focusing the femtosecond laser is needed as its  $1/e^2$  diameter of it before entering the main chamber is 4 mm. Normally one can use a focusing lens in front of the main chamber. However, in this case, the focal length will reach at least 310 mm, which will result in a Rayleigh length of 12.24 mm and this has negative effect on momentum resolution. Thus, in our setup, a concave mirror with a focal length of  $f = 75$  mm is set on the opposite side of the incident direction of the femtosecond laser propagation which can focus the light to a  $1/e^2$  diameter of 19.10  $\mu\text{m}$  at the target regime. In this way, the Rayleigh length is decreased to 716.20  $\mu\text{m}$ , and the resolution of recoil ion momentum due to target size can be neglected. Besides, the density profile of 3D MOT is measured by scanning it, which means the ionizing focus center should be adjusted accurately. Thus, the focusing lens is mounted on a multi-axis manipulator and two pairs of adding coils are mounted on the directions of 2D beam and spectrometer longitude. The manipulator has a travel range of 75 mm in the direction of femtosecond laser propagation and 16 mm in either of the other two directions. However, as the theoretical resolution of the manipulator movement is only 0.5 mm which is not enough for characterization of our target, thus we use two additional pairs of coils to move the target instead of move the ionization laser, the characterization will be described later. The trapping center of the 3D MOT will be moved by the magnetic field generated by the adding coils. By change the current of the coils, the 3D MOT target is measured to move linearly and the scale coefficient is 1.040 mm/A in the direction of 2D beam and 0.625 mm/A in the direction of spectrometer longitude. Based on the minimum incremental step of 0.01 A of our power supply, the resolution of the shift distance can reach 6.25  $\mu\text{m}$  and 10.40  $\mu\text{m}$  in each direction, respectively. By using both the manipulator and the additional coils, a sufficient travel range and a suitable shift distance are satisfied simultaneously. Then, according to the relationship between the magnetic field gradient and ionization rate, the magnetic field gradient is optimized at 18 G/cm by applying a current of 47 A to the coils to obtain the highest atom density. The ionization rate is proportional to the atom number in the focus volume of ionization laser, i.e. a high ionization rate means a high atom target density. Thus, by scanning the ionization laser along the center lines of the cold

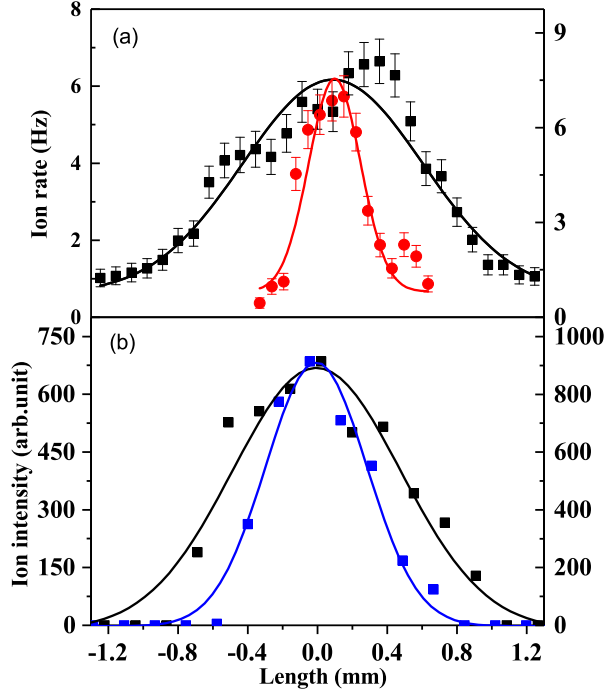


FIG. 3. Cold atom target density profile measured by (a) photoionization experiment in the direction of spectrometer longitude (black square) and 2D beam (red spot) and (b) absorption experiment in the directions of spectrometer longitude (black square) and femtosecond laser propagation (blue triangle). All curves are corresponding data fitting to Gaussian functions.

atom target in the directions of spectrometer longitude and 2D beam via the method of controlling the manipulator and the current flow through the adding coils, the density profile of 3D MOT atom target in corresponding directions can be obtained. The target density profile is scanned with a step of 0.0625 mm in the direction of spectrometer longitude and 0.052 mm in the direction of 2D beam as shown in Fig. 3(a). The black square and the red spot correspond to the ionization rate in specific position of different directions. Fitting the data to Gaussian functions, which are shown as black curve and red curve in Fig. 3(a), the profiles of the atom target in the two directions are obtained. The target width on the two directions, i.e. the FWHMs of the Gaussian fitted curves, are 1.221 mm and 0.349 mm, respectively.

The density profile of cold atom target is also measured by absorption imaging experiment. Illuminating the 3D MOT atom target by an imaging laser beam which is resonant with the cold atom. The imaging laser beam is transported from the top of the main chamber, then a CMOS camera is set at the bottom. The CMOS camera can image the shadow of the illumination light absorbed by the atom target. As the absorption imaging optical system is set at the bottom, only the density profile in the directions of spectrometer longitude and femtosec-

ond laser propagation can be measured. As shown in Fig. 3(b), the black square and the blue triangle corresponding to the atom density in specific position along with the two center lines of the mentioned directions in the horizontal plane of the atom target by equal intervals. The black curve and the blue curve are Gaussian functions fitted to the black square and the blue circle, respectively. The FWHMs of the Gaussian fitted curves are 1.138 mm and 0.683 mm.

Using the method of absorption imaging, the velocity in the directions of spectrometer longitude and femtosecond laser propagation are also deduced which are 0.113 m/s and 0.116 m/s, corresponding to atom temperature 128  $\mu$ K and 132  $\mu$ K. Besides, the atom density of the target is about  $10^8 \sim 10^9$  /cm<sup>3</sup> in this situation. Additionally, as the atom density is in proportion to the ion rate when the targets interact with the same femtosecond laser, the order of magnitude of atom densities of molasses and 2D MOT are  $10^8$  and  $10^7$ , respectively.

Depending on the density of cold atoms target needed in specific experiments, different magnetic field gradient could be generated by fixing the detuning of cooling and repumping laser then changing the current passing through the coils. With specific ionization intensity, the atom density is proportion with the ionization rate under different magnetic field gradient. The relationship between photoionization rate and magnetic field gradient is measured and the result is shown in Fig. 4. The photoionization rate grows linearly with the magnetic field gradient in the range of 6 G/cm to 15 G/cm approximately. It is difficult to form 3D MOT atom target under the condition of the magnetic field gradient lower than 6 G/cm, so the ionization rate increasing slowly with the increasing of magnetic field gradient. In the range of magnetic field gradient higher than 15 G/cm, the photoionization rate tends to stable at 120 Hz. According to the result of the relationship between the photoionization rate and the magnetic field gradient, different type of experiment can be performed with expected density of cold atom target. It should be note that increasing the ionization laser intensity, the ionization rate will increase entirely but with the same variation tendency.

Based on the understanding of the cold atom target mentioned above, photoionization experiments are performed to obtain more information about different target types. Fig. 5(a),(b) and (c) have shown the recoil ion momentum spectra for photoionization in the xy-plane of the detector of three atom target types, calculated by the position on the detector and the corresponding time of flight. The recoil ion momentum distribution of different targets in two orthogonal directions has been plot in one figure respectively. In Fig. 5(d)  $p_x$  represent for the recoil ion momentum in the direction of 2D beam. Since both the 3D MOT atom target and the molasses atom target are further cooled by cooling laser in three directions in the main chamber, their FWHM of recoil ion momentum are similar in x-axis. But the 2D MOT atom target is only pre-cooled in two dimensions and pushed in

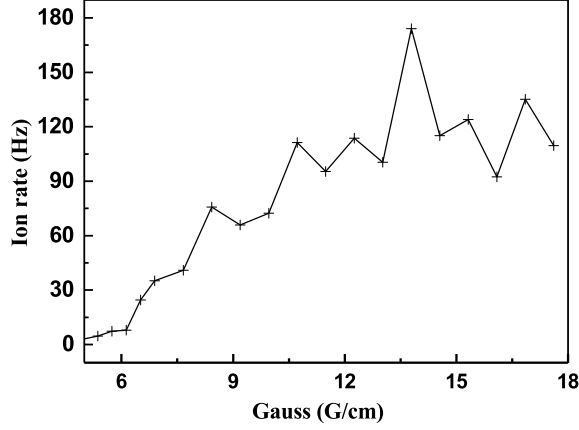


FIG. 4. Relationship between magnetic field gradient and ion rate.

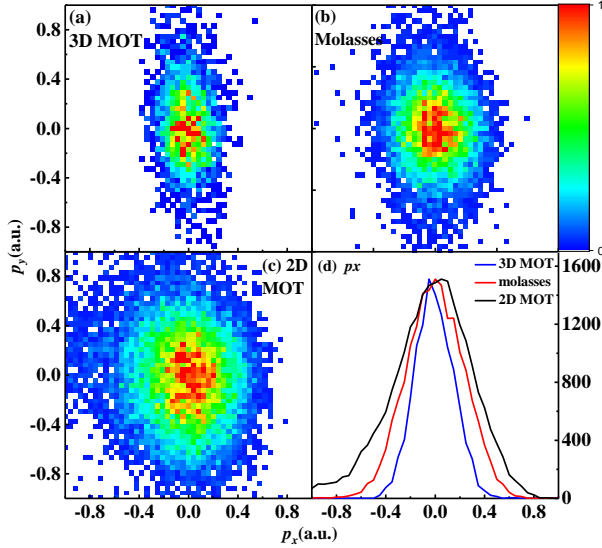


FIG. 5. Momentum distribution on the xy-plane of (a) 3D MOT target, (b) molasses target and (c) 2D MOT target. (d) Momentum distribution on the vertical direction of three types of targets.

the main chamber, so its FWHM of recoil ion momentum spectra is larger than the other two. The FWHM recoil ion momentum in the direction of femtosecond laser propagation ( $p_y$  in Figures) are about 1.4 times larger than that in the direction of 2D beam in all types of atom targets, respectively, which are caused by the Rayleigh range of the ionization laser. The Rayleigh range of the ionization laser is  $716.20 \mu\text{m}$  which is much larger than its waist diameter of  $19.10 \mu\text{m}$ .

#### IV. RESULT

The recoil ion momentum distribution in the directions of spectrometer longitude and 2D beam of the 3D MOT target of the experiment and the theory calculation are shown in Fig. 6(a) and (b), respectively. And in Fig. 6(c) the recoil ion momentum distribution in the direction of spectrometer longitude of the 3D MOT atom targets and the theory calculation are compared. The experimental data in Fig. 6(b) has been sliced  $p_y$  in the range of  $-0.2 \text{ a.u.} \sim 0.2 \text{ a.u.}$  and the experimental and theoretical data in Fig. 6(c) have been sliced  $\sqrt{p_x^2 + p_y^2}$  in the range of  $0 \sim 0.2 \text{ a.u.}$

According to the experiment parameters, the Keldysh parameter  $\gamma$  is 45, which means the photoionization process in our experiment is multiphoton ionization. With the method of single-active electron approximation (SEA), assuming that the rest of the electrons are frozen in the atom, the generation of the harmonic can be attributed to the effect of ion binding potential and the motion of a valence electron in the laser field. The process of the electrons bound by bound potential energy  $V(r)$  from ground state  $|0\rangle$  scattering through an external laser field to continuous state  $|p\rangle$  can be describe by quantum scattering matrix theory. By this theoretical framework, the strong field approximation (SFA) theory<sup>23-25</sup> is used to describe the motion of the electrons in the laser field based on the Volkov state, as the effect of the strong laser field in electron is much larger than that of the nucleus electron. Thus, the approximate transition amplitude expression is obtained with the model that the electron transitions from the ground state to the continues state of Volkov directly.

In the calculation, the intensity of ionization laser is set at  $10^{10} \text{ W/cm}^2$ , and there are 20 optical cycles in one laser pulse which mean the pulse width is 26 fs. Then using the data calculated with SFA as signal data (blue curve in Fig. 6(c)), the convolution algorithm is applied with a Gaussian function of  $\text{FWHM} = 0.15$  as instrumental response function (IRF). With the comparison of the experimental and theoretical calculation results, an upper limit resolution of recoil ion momentum of  $0.15 \text{ a.u.}$  has been obtained.

Additional, different atom targets have a similar difference momentum in direction of spectrometer longitude which means that the momentum resolution of three types of target are the same in this direction. It is necessary to mention that the number of ions ionized by the same intensity of ionization laser in one pulse in different target types, 2D MOT, molasses, or 3D MOT, are different because different type of target has different atom density. However, when the number of ions is larger than one, there will be space charge effect which has negative effect on the resolution of recoil ion momentum. Thus, we control the power of ionization laser as high as possible to get a higher experiment efficiency but avoid photoionization more than one ion. Specially, the intensity of the



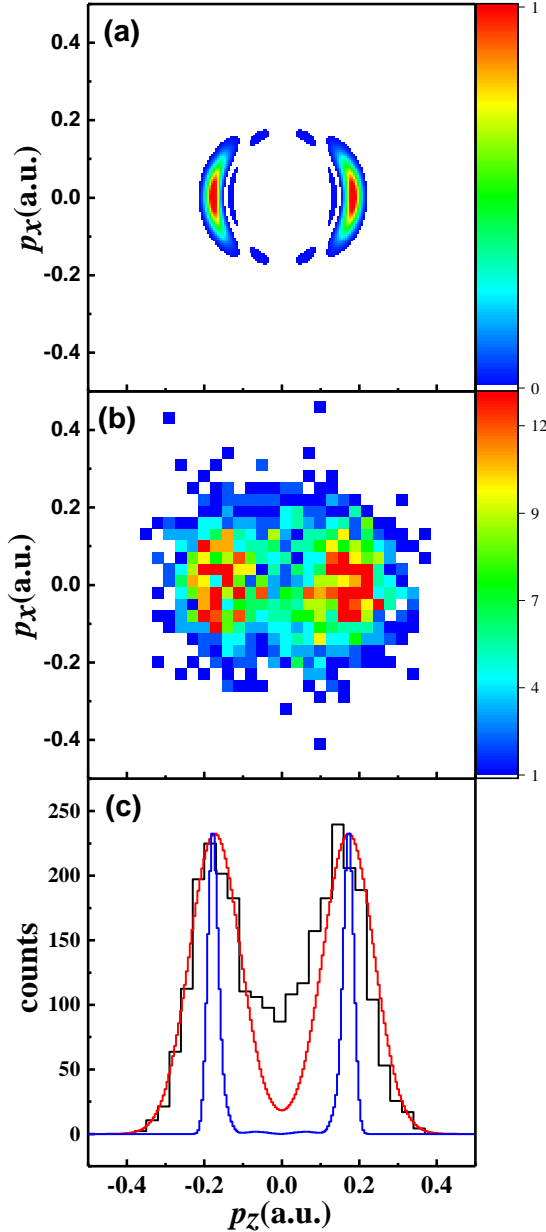


FIG. 6. Recoil ion momentum distribution in the directions of spectrometer longitude and 2D MOT (a) SFA theory calculation and (b) experimental data. (c) Comparison of the recoil ion momentum distribution in the direction of spectrometer longitude of 3D MOT targets experiment data (black curve) SFA theory calculation (blue curve) and the theory result with convolution (red curve). The data in (b) and (c) have been sliced.

femtosecond laser beam are  $8 \times 10^{11}$  W/cm<sup>2</sup>,  $1 \times 10^{11}$  W/cm<sup>2</sup> and  $2 \times 10^{10}$  W/cm<sup>2</sup> for 2D MOT, molasses and 3D MOT target, respectively, which corresponding to the Keldysh parameters of 6, 19 and 45. Though the powers of ionization laser beams are different in different targets, the ionization process in our experiments are all carry on in the region of multiphoton ionization according to

the Keldysh Theory. Thus, it is reasonable to compare them with each other. Besides, experiment of switch off the magnetic coils current during the data acquisition to avoid the influence of magnetic field are performed. The result is obtained that the magnetic field has little effect on the resolution of recoil ion momentum which also can be corrected by data analysis. However, switch off the magnetic coil current and rebuild the 3D MOT target will cost more than 20 times as much time as experiment without this process. Thus, there is no need to switch off the magnetic coil current in our experiment.

## V. CONCLUSION

We have designed and tested a new MOTRIMS apparatus which can be worked in three types of atom targets, in molasses, 2D MOT, and 3D MOT. Different density of cold atom target can be prepared in the setup fitting variety of experiment include photoionization experiments of light of different wavelength or different intensity and ion-atom collision experiments of different ion species. In 3D MOT, the cold atom target has been characterized by absorption imaging experiments in size, velocity, temperature and the relationship between its density and the magnetic field gradient. An atom target density of  $3 \times 10^8$  /cm<sup>3</sup> has been obtained in which situation the temperature of the atom target has reached  $\sim 100$   $\mu$ K, corresponding to velocity of  $\sim 0.1$  m/s. Meanwhile, the 3D MOT atom target size is measured by photoionization experiment as well which can validate the result obtained from absorption imaging experiment. In the present work, all the photoionization experiments are performed with femtosecond laser with a wavelength of 800 nm and a repetition of 1 kHz. For getting a focused ionization laser of better quality, we set a concave mirror inside the main chamber with shorter Rayleigh range than using a focusing lens outside the main chamber. The recoil ion spectrum in different directions in three types of atom targets have been measured. We got a result that the resolution of recoil ion momentum is similar for atom target in molasses and in 3D MOT. Thus, photoionization experiment can be operated either in molasses with lower atom target density or in 3D MOT with higher atom target density without considering the difference of the resolution of recoil ion momentum. For some experiments low atom target density but has no demand on high resolution of momentum is needed, such as some ion-atom collisions with typical momenta transfer on the order of 10 a.u., 2D MOT will also be a suitable cold atom target. All these data offered important information that what kinds of experiments can be operated in this setup. The further experiments of our setup will be focus on the investigation of the interaction process between the mid-infrared laser and cold rubidium.

<sup>1</sup>R. Dörner, J. Ullrich, H. Schmidt-Böcking, and R. E. Olson, Phys. Rev. Lett. **63**, 147 (1989).

- <sup>2</sup>J. Ullrich, R. Dörner, S. Lencinas, O. Jagutzki, H. Schmidt-Böcking, and U. Buck, *Nuclear Instruments and Methods in Physics Research Section B: Beam Interactions with Materials and Atoms* **61**, 415 (1991).
- <sup>3</sup>R. Moshhammer, J. Ullrich, M. Unverzagt, W. Schmidt, P. Jardin, R. E. Olson, R. Mann, R. Dörner, V. Mergel, U. Buck, and H. Schmidt-Böcking, *Phys. Rev. Lett.* **73**, 3371 (1994).
- <sup>4</sup>Y. Huismans, A. Rouzée, A. Gijsbertsen, J. H. Jungmann, A. S. Smolkowska, P. S. W. M. Logman, F. Lépine, C. Cauchy, S. Zamith, T. Marchenko, J. M. Bakker, G. Berden, B. Redlich, A. F. G. van der Meer, H. G. Muller, W. Vermin, K. J. Schafer, M. Spanner, M. Y. Ivanov, O. Smirnova, D. Bauer, S. V. Popruzhenko, and M. J. J. Vrakking, *Science* **331**, 61 (2011), <http://science.sciencemag.org/content/331/6013/61.full.pdf>.
- <sup>5</sup>B. DePaola, R. Morgenstern, and N. Andersen (Academic Press, 2008) pp. 139 – 189.
- <sup>6</sup>M. Schuricke, G. Zhu, J. Steinmann, K. Simeonidis, I. Ivanov, A. Kheifets, A. N. Grum-Grzhimailo, K. Bartschat, A. Dorn, and J. Ullrich, *Phys. Rev. A* **83**, 023413 (2011).
- <sup>7</sup>G. Zhu, M. Schuricke, J. Steinmann, J. Albrecht, J. Ullrich, I. Ben-Itzhak, T. J. M. Zouros, J. Colgan, M. S. Pindzola, and A. Dorn, *Phys. Rev. Lett.* **103**, 103008 (2009).
- <sup>8</sup>M. Schuricke, G. Zhu, J. Steinmann, K. Simeonidis, I. Ivanov, A. Kheifets, A. N. Grum-Grzhimailo, K. Bartschat, A. Dorn, and J. Ullrich, *Phys. Rev. A* **83**, 023413 (2011).
- <sup>9</sup>D. Fischer, D. Globig, J. Goullon, M. Grieser, R. Hubele, V. L. B. de Jesus, A. Kelkar, A. LaForge, H. Lindenblatt, D. Misra, B. Najjari, K. Schneider, M. Schulz, M. Sell, and X. Wang, *Phys. Rev. Lett.* **109**, 113202 (2012).
- <sup>10</sup>W. Salzmann, T. Mullins, J. Eng, M. Albert, R. Wester, M. Weidemüller, A. Merli, S. M. Weber, F. Sauer, M. Plewicky, F. Weise, L. Wöste, and A. Lindinger, *Phys. Rev. Lett.* **100**, 233003 (2008).
- <sup>11</sup>S. Gtz, B. Höltkemeier, C. S. Hofmann, D. Litsch, B. D. DePaola, and M. Weidemüller, *Review of Scientific Instruments* **83**, 073112 (2012), <https://doi.org/10.1063/1.4738643>.
- <sup>12</sup>S. Gtz, B. Höltkemeier, T. Amthor, and M. Weidemüller, *Review of Scientific Instruments* **84**, 043107 (2013), <https://doi.org/10.1063/1.4795475>.
- <sup>13</sup>S. Weyers, E. Aucouturier, C. Valentin, and N. Dimarcq, *Optics Communications* **143**, 30 (1997).
- <sup>14</sup>T. G. Tiecke, S. D. Gensemer, A. Ludewig, and J. T. M. Walraven, *Phys. Rev. A* **80**, 013409 (2009).
- <sup>15</sup>J. Schoser, A. Batär, R. Löw, V. Schweikhard, A. Grabowski, Y. B. Ovchinnikov, and T. Pfau, *Phys. Rev. A* **66**, 023410 (2002).
- <sup>16</sup>Z. T. Lu, K. L. Corwin, M. J. Renn, M. H. Anderson, E. A. Cornell, and C. E. Wieman, *Phys. Rev. Lett.* **77**, 3331 (1996).
- <sup>17</sup>K. Dieckmann, R. J. C. Spreeuw, M. Weidemüller, and J. T. M. Walraven, *Phys. Rev. A* **58**, 3891 (1998).
- <sup>18</sup>J. Catani, P. Maioli, L. De Sarlo, F. Minardi, and M. Inguscio, *Phys. Rev. A* **73**, 033415 (2006).
- <sup>19</sup>H. Nguyen, X. Fléhard, R. Brdy, H. A. Camp, and B. D. DePaola, *Review of Scientific Instruments* **75**, 2638 (2004), <https://doi.org/10.1063/1.1775310>.
- <sup>20</sup>J. Blicke, X. Fléhard, A. Cassimi, H. Gilles, S. Girard, and D. Hennecart, *Review of Scientific Instruments* **79**, 103102 (2008), <https://doi.org/10.1063/1.2994151>.
- <sup>21</sup>D. W. Preston, *American Journal of Physics* **64**, 1432 (1996), <https://doi.org/10.1119/1.18457>.
- <sup>22</sup>C. J. Dedman, J. Nes, T. M. Hanna, R. G. Dall, K. G. H. Baldwin, and A. G. Truscott, *Review of Scientific Instruments* **75**, 5136 (2004), <https://doi.org/10.1063/1.1820524>.
- <sup>23</sup>W. Ketterle, D. S. Durfee, and D. M. Stamper-Kurn, *Physics* (1999).
- <sup>24</sup>L. V. KELDYSH, *Sov Phys* **20** (1965).
- <sup>25</sup>F. H. M. Faisal, *Journal of Physics B: Atomic and Molecular Physics* **6**, L89 (1973).